LA-UR -91-3870

Los Alamos National Laboratory is operated by the University of California for the United States Department of Energy under contract W-7405-ENG-36

TITLE   **ELECTROMAGNETIC IMAGING OF DYNAMIC BRAIN ACTIVITY**

AUTHOR(S):   J. Mosher, (Univ of Southern California, USC)
P. Lewis, MEE-3
J. Lewine, P-6
J. George, P-6
R. Leahy, USC
M. Singh, USC

Los Alamos Los Alamos National Laboratory
Los Alamos, New Mexico 87545

Electromagnetic Imaging of Dynamic Brain Activity*

J. Mosher*, P. Lewis†, J. Lewine‡, J. George‡, R. Leahy*, M. Singh+

*Signal & Image Processing Institute
Dept. Electrical Engineering-Systems
University of Southern California
Los Angeles. CA 90089-2564

†Los Alamos National Laboratory
Mechanical & Electronic Engineering Division
Group MEE-3, MS J580
Los Alamos. NM 87545

+Department of Radiology
University of Southern California
1985 Zonal Ave. PSC-610
Los Angeles, CA 90033

‡Los Alamos National Laboratory
Physics Division
Group P-6, MS M715
Los Alamos, NM 87545

Abstract

Neural activity in the brain produces weak dynamic electromagnetic fields that can be measured by an array of sensors. Using a spatio-temporal modeling framework, we have developed a new approach to localization of multiple neural sources. This approach is based on the MUSIC algorithm originally developed for estimating the direction of arrival of signals impinging on a sensor array. We present applications of this technique to magnetic field measurements of a phantom and of a human evoked somatosensory response. The results of the somatosensory localization are mapped onto the brain anatomy obtained from magnetic resonance images.

I. Introduction

Technological advances over the past two decades have created high-resolution techniques, such as magnetic resonance imaging, for noninvasive imaging of the anatomical structure of the brain. Techniques for imaging the *functional* activity of the brain are less advanced, and no single technique can provide adequate spatial and temporal resolution. For example, positron emission tomography provides high spatial resolution but poor temporal resolution, while conventional electroencephalography (EEG) provides high temporal resolution but poor spatial resolution.

Current flow caused by neuronal activity produces electromagnetic fields that can be measured outside of the head. These electromagnetic fields, measured at many points on the head by an array of sensors, provide the basis of our approach to functional imaging. In the most general form, the neural electromagnetic inverse problem is ill-posed and has no unique solution[1, 2]. However, by employing source models it is possible to solve the in-

verse problem for certain classes of neural activity, such as the early response to an external stimulation. Present methods are based on *static* field analysis, which limits the complexity of neuronal activity that can be examined. To overcome these limitations, we have extended the analysis to the temporal domain by casting the problem in the framework of sensor array signal processing and adapting techniques developed in sensor array applications, such as acoustic, radar, and seismic signal processing.

Our approach to functional imaging is based on MUSIC (MUltiple Source Identification and Classification), an algorithm originally developed for determining the direction of arrival of signals impinging upon a sensor array[3]. We have extended the algorithm to apply to neuromagnetic measurements (magnetoencephalography or MEG) and/or neuroelectric measurements (EEG). This approach analyzes both the spatial and temporal aspects of the field measurements. Using an eigenvalue analysis of the spatial/temporal measurements, MUSIC identifies a signal subspace. A virtual "test" source is then scanned throughout the volume of the brain to look for geometric intersections between the field patterns produced by the source and the signal subspace. The resulting three dimensional volumetric scan can be easily correlated to and/or constrained by anatomical structural imagery. Once the locations of the active neural regions are determined from this scan, the corresponding temporal activation patterns can be found by a linear least squares fit.

II. MEG/EEG MUSIC Algorithm

In this section we briefly describe the MEG/EEG MUSIC algorithm. More thorough treatments may be found in references [4, 5, 6, 7]. For simplicity, we treat the case of radial magnetic measurements outside of a head modeled as a spherically symmetric conductor. Neural sources are modeled as current dipoles. Although the example is specific, the same general approach can be applied to a wide variety of source and head models in both MEG and EEG.

Using the Biot-Savart law and a head-centered coordinate system, the radial component of the external magnetic

field generated by a current dipole source can be expressed as [8]

$$B \; \doteq \; \frac{\mu_o}{4\pi} \frac{(\vec{R} - \vec{L}) \times \vec{R}}{|\vec{R} - \vec{L}|^3 |\vec{R}|} \cdot \widehat{M} S \qquad (1)$$

$$= \; \vec{g}(\vec{L}) \cdot \widehat{M} S \; . \qquad (2)$$

B is the radial field strength at location $\vec{R}$ outside of the head. S is the strength and $\widehat{M}$ the unit vector moment (or orientation) of the current dipole source located at $\vec{L}$ inside the head. The defined $\vec{g}(\vec{L})$ is a gain vector, relating the moment intensity of the dipole to the external field. Due to the geometry of this model, only the two tangential components of $\widehat{M}$ produce external radial magnetic fields.

Using m measurement locations and expressing $\vec{g}(\vec{L})$ as a 1×2 row vector, we can stack the gain vectors for a single source i to form an $m \times 2$ gain matrix $\mathbf{G}_i$, that specifies the radial fields produced by each of the two tangential components of the source. If $\widehat{M}$ is expressed as a 2×1 column vector, then the overall radial field produced by source i is $\mathbf{G}_i \widehat{M}_i$. The temporal dimension is added to our model by fixing the source locations and orientations— $\mathbf{G}$ and $\widehat{M}$ are time invariant. (See references [4, 5] for a treatment of time-varying orientation.) The time-varying magnetic field measurements produced by p sources can then be expressed as

$$\underline{E}(t) \; = \; \left[\mathbf{G}_1 \widehat{M}_1 \cdots \mathbf{G}_p \widehat{M}_p \right] \left[\begin{array}{c} S_1(t) \\ \vdots \\ S_p(t) \end{array} \right] + \underline{N}(t) \quad (3)$$

$$= \; \mathbf{G} \underline{S}(t) + \underline{N}(t) \qquad (4)$$

where $\underline{E}(t)$ is the $m \times 1$ vector of measurements, $S(t)$ denotes the dipole magnitude, and $\underline{N}(t)$ represents the additive noise or measurement error.

Fundamental to the MUSIC approach is the concept of *signal subspace*. From (4) we know that any "perfect" field measurement, uncorrupted by noise, would lie in the column space or signal subspace of the gain matrix $\mathbf{G}$. Although the signal subspace is not known *a priori*, it is estimated from successive measurement "snapshots" using the singular value decomposition [9]. Furthermore, in the absence of "array ambiguities," the only sources whose fields can lie in the signal subspace are the true sources. Hence, once the signal subspace is known, the *multiple source* localization problem reduces to the geometric problem of determining which single source fields lie within the signal subspace. This is accomplished by an exhaustive scan of a *single source* over all possible locations.

At each candidate source location $\vec{L}$, a measure $J(\vec{L})$ of the intersection between the signal subspace and the source gain is computed and scaled between zero and one, with a value of one indicating a perfect intersection. These intersection points correspond to the underlying source locations. In summary, the MEG/EEG MUSIC algorithm consists of the following steps:
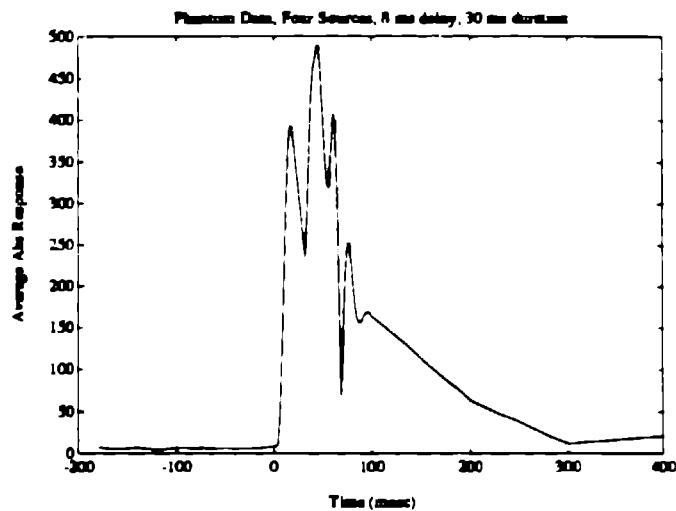
1 From a set of successive field measurements, use the singular value decomposition to estimate the number of sources and to characterize the signal subspace.

2 At each point $\vec{L}$ on a fine grid of three-dimensional locations, compute the intersection measure $J(\vec{L})$ between the signal subspace and the gain or forward field produced by a source at that location.

3 Identify source locations from the maxima of the intersection measure where $J(\vec{L})$ approach one.

4 Optionally refine the location estimates by using a finer grid in source areas.

5 For each source, compute the orientation $\widehat{M}$ and activation time course $S(t)$ [4].

III. Phantom Data Results

A seven-sensor, 2nd-order gradiometer system was placed in six different positions about a glass sphere of radius 9 cm, for a total of 42 measurement locations. Four dipole sources were placed inside the sphere, which was filled with a conducting solution. The sources were doubly shielded coaxial cables, with the inner conductor extending 2 mm beyond its inner coaxial sheath. The sources were located within the sphere to an accuracy of approximately ±3 mm.

In Figure 1, which displays the average absolute response recorded over all sensors, we see the overlap between the source responses. Each source produced an approximately 30 ms wide monopulse, with each source firing about 8 ms after the previous, such that the fourth source was activated before the first source had completed its response.
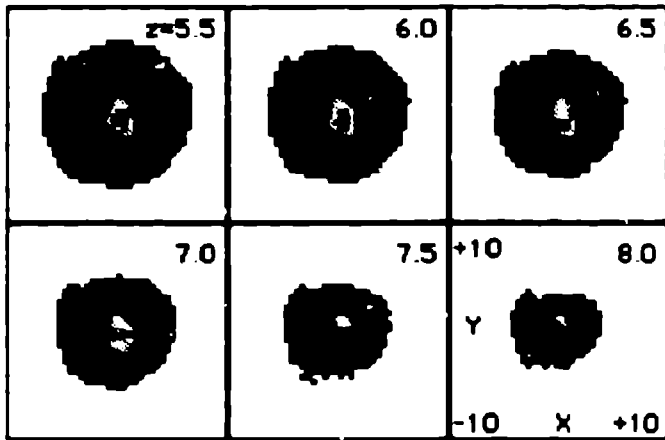
Fig 2 Phantom data - Six axial slices of the initial 5 mm MUSIC scan with peaks darkened for clarity Slices run from :=55 to :=80 cm and each slice spans ±10 cm in the x and y directions

Using the MUSIC algorithm, the data set was scanned over a 20 cm source cube at a 0.5 cm sample interval to establish the overall quality of the data and to confirm the absence of ambiguous head regions The scan results were examined by converting the three dimensional metric information into two dimensional slices In Figure 2 we show six axial slices from the initial 5 mm MUSIC scan

Using the 5 mm scan result, a smaller region was selected and scanned at a 1 mm interval and the results also displayed as slices From these slices three "peaks" (points where the metric approached one) were identified In Figure 3 we show nine axial slices from the 1 mm MUSIC scan, with each set of three spanning an identified source location

The locations of the MUSIC scan peaks are given in Table I. along with the true source locations Sources 2 and 4 were well resolved, as indicated by the narrow peaks in both figures and the good agreement with the true locations The other source that was identified had a much broader peak that spans the region near Sources 1 and 3. indicating that these two closely spaced sources may not be resolvable by this array configuration Indeed. the three sources identified explain 99 percent of the data variance Repetitions of this experiment could be conducted to determine the variance of these results

IV. Somatosensory Data Results

In this experiment the neuromagnetic fields of the evoked response were collected for three cases. Thumb stimulation of the thumb, Ring stimulation of the ring finger, and Both simultaneous stimulation of both digits The data were generated by vibrotactile stimulation using a piezoelectric speaker element The intent was that
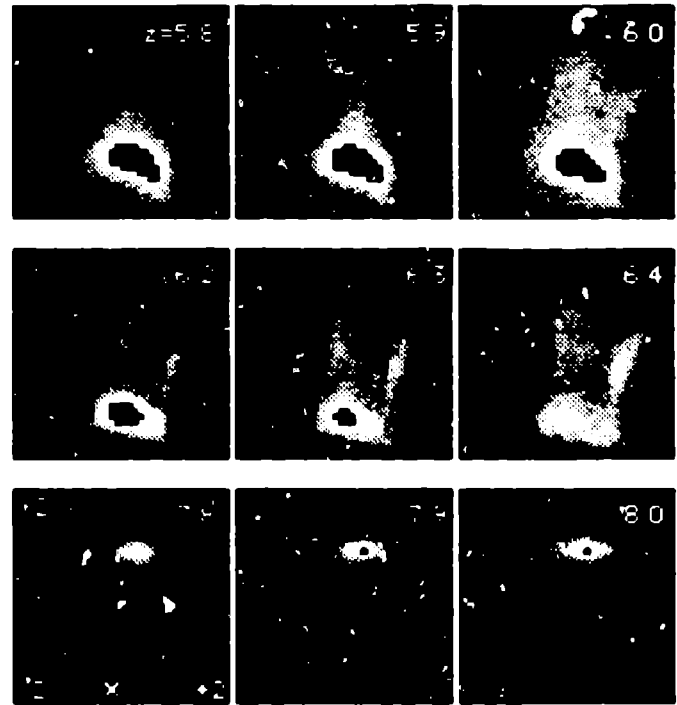

Fig 3 Phantom data - Nine axial slices of the final 1 mm MUSIC scan with peaks darkened for clarity Slices span ±2 cm in the x and y directions The top set spans the first source location with slices at :=5.8, 5 9. and 6 0 cm The middle set spans the second source at :=6 2, 6 3. and 6 4 cm The bottom set spans the fourth source at :=7 7. 7 8. and 7 9 cm

source	True Loc (±0 3 cm)	MUSIC Loc (0 1 cm grid)	Loc. Error (cm)
x	0 16	0 2	
(1) y	-0 82	-1 0	0 2
z	5 90	5 9	
x	0 HH	0 9	
(2) y	-0 2H	-0 4	0 2
z	6 30	6 5	
x	-0 15		
(3) y	-0 30		
z	5 20		
x	0 27	0 3	
(4) y	0 H1	0 H	0 1
z	7 75	7 H	
var %	99 4	9H 9	

Table I Comparison on MUSIC localization results with true locations
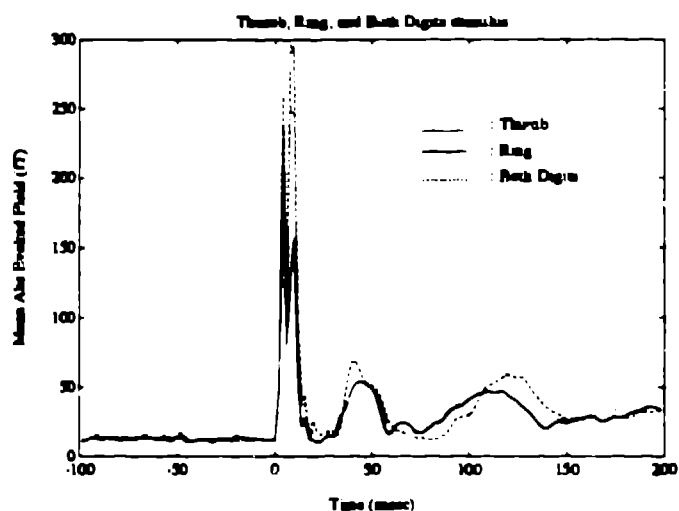
Fig 4 Average absolute evoked field from somatosensory stimulus

Fig 5 Somatosensory data - Three slices of the 5 mm MUSIC scan for the *both* case with peaks darkened for clarity Slices shown are for $z=6.5$, 7.0, and 7.5 cm and each spans ± 10 cm in the x and y directions

	x	y	z
Both	0.5	4.3	6.9
Ring	0.8	4.1	7.5
Thumb	0.6	4.5	7.2

Table II MUSIC locations of the somatosensory piezo-electric stimulations

the *both* field pattern might reflect a summation of the individual *ring* and *thumb* fields The data were collected during eleven placements of a seven-sensor, 2nd-order gradiometer system, for a total of 77 sensor locations Data were filtered online between 1 and 100 Hz and sampled at a 1 kHz rate At each placement 300 trials were averaged for each stimulus Figure 4 plots the average of the absolute response across all of the sensors Since piezoelectric stimulation creates a large stimulus artifact, only the data after 24 msec were processed

To locate the general area of neural activity, initial MUSIC scans were performed for all three cases on a 5 mm grid Figure 5 shows three slices from the *both* case Finer, 1 mm scans were then performed Figure 6 shows three slices from each case, spanning the area of activation Table II displays the coordinates of the peaks located in these scans Figure 7 shows the anatomical location of the source found from the *thumb* MUSIC scan This source lies along the posterior bank of the central sulcus, consistent with the expected anatomical locus The *ring* and *both* source locations also lie in this same anatomical region

We note from Table II and Figure 6 that there is a distinct shift between the *thumb* and *ring* responses The *both* response has a much broader peak that encompasses the peaks found in the separate *thumb* and *ring* responses All
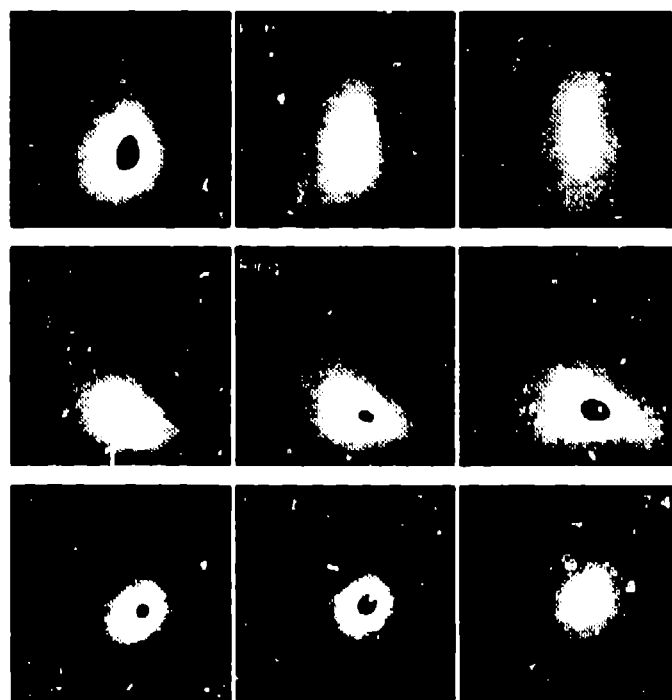

Fig 6 Somatosensory data - Nine slices of the 1 mm MUSIC scans with peaks darkened for clarity From top row to bottom row the slices are from the *both*, *ring*, and *thumb* cases Slices shown are for $z=7.0$, 7.2, and 7.4 cm and each spans the x-axis horizontally from -2.0 to 2.0 cm and the y-axis vertically from 3.0 to 7.0 cm
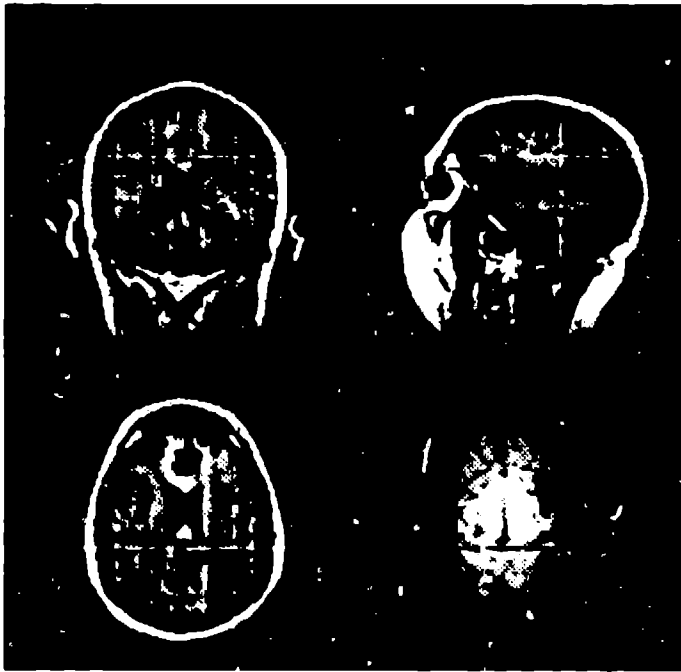
Fig 7 MUSIC source location of the *thumb* response in MRI scans of the subject

three scans exhibit broader MUSIC peaks than the phantom data These broader peaks may be due to modeling errors, since the dipole source and spherical head model used are a better physical match to the phantom than to a human head

References

[1] S J Williamson, G -L Romani, L Kaufman, and I Modena, eds, *Biomagnetism An Interdisciplinary Approach* New York Plenum Press, 1983

[2] B Jeffs, R Leahy, and M Singh, "An evaluation of methods for neuromagnetic image reconstruction" *IEEE Trans Biomedical Engineering* BME-34(713 723) Sept 1987

[3] R O Schmidt, "Multiple emitter location and signal parameter estimation," *IEEE Trans Antennas and Propagation*, AP-34(276 280), March 1986

[4] J C Mosher, P S Lewis, and R Leahy "Multiple Dipole Modeling and Localization from Spatio-temporal MEG Data," *IEEE Trans Biomedical Engineering* (in press) 1991

[5] J C Mosher, P S Lewis, and R Leahy "Subspace methods for identifying neural activity from electromagnetic measurements of the brain" *Proc 25th Asilomar Conf on Signals, Systems, and Computers* (in press) IEEE Pacific Grove, CA, Nov 1991

[6] J C Mosher, P S Lewis, R Leahy, and M Singh "Multiple dipole modeling of spatio-temporal MEG data," in *Digital Image Synthesis and Inverse Optics* (A F Gmitro, et al eds.), pp. 364-375 Proc SPIE 1351, San Diego, CA July 1990

[7] J C Mosher, P S Lewis, and R Leahy, "Spatial localization of neural sources using the magnetoencephalogram," *Fifth ASSP Wkshp on Spectrum Estimation and Modeling* pp 289-293, Rochester, NY Oct 1990

[8] J Sarvas, "Basic mathematical and electromagnetic concepts of the biomagnetic inverse problem," *Physics Medical Biology*, 32 1(11 22), 1987

[9] J A Cadzow, "Multiple source location – The signal subspace approach," *IEEE Trans on Acoustics, Speech and Signal Processing*, ASSP-38(1110 1125), July 1990